Available online at www.sciencedirect.com
ScienceDirect
Journal of the European Ceramic Society 29 (2009) 411–418
www.elsevier.com/locate/jeurceramsoc

Ionic conductivity of tetragonal ZrO_2 polycrystal doped with TiO_2 and GeO_2

Hidehiro Yoshida *, Koji Morita, Byung-Nam Kim, Keijiro Hiraga

National Institute for Materials Science, 1-2-1 Sengen, Tsukuba, Ibaraki 305-0047, Japan

Received 13 March 2008; received in revised form 20 June 2008; accepted 23 June 2008
Available online 26 July 2008

Abstract

The effects of the co-doping and the resultant co-segregation of 2 mol% TiO_2 and 2 mol% GeO_2 on the ionic conductivity and on the chemical bonding state in a tetragonal ZrO_2 polycrystal were investigated. The conductivity data and grain boundary microstructure showed that the doped Ti^{4+} and Ge^{4+} cations segregate along the grain boundary, and this segregation causes a reduction in the conductivity of both the grain interior and grain boundary and an increase in the activation energy of the grain boundary conductivity. Overall, the data indicate that the segregation retards the diffusion of oxygen anions. A first-principle molecular orbital calculation explains the retarded diffusion of the oxygen anion from a change in the covalent bonds around the dopant cations; an increase in the strength of the covalent bond between the oxygen and doped cation should work to suppress the diffusion of the oxygen anion.

Keywords: Grain boundaries; Impurities; Ionic conductivity; ZrO2; Molecular orbital calculation

1. Introduction

Recent studies[1–4] on yttria-stabilized tetragonal zirconia polycrystals (Y-TZP) have shown that grain boundary matter transport in TZP is highly sensitive to a small amount of cation doping on a level of only a few mol% or less. A typical example is the high temperature superplastic flow in TZP.[1–4] Studies showed that the flow stress in the superplastic TZP strongly depends on the type of doping cations, and the co-doping of TiO_2 and GeO_2 is particularly effective for enhancing the superplasticity, namely, reducing the level of flow stress and increasing the tensile ductility.[3] Such a doping effect can be explained by the increase in the grain boundary diffusivity of the Zr^{4+} cation, because a couple of grain boundary sliding and grain switching accommodated by the grain boundary diffusion of the Zr^{4+} cation can be regarded as the main mechanism of the superplastic flow in TZP.[5–7]

In order to know the origin of the doping effect on the grain boundary diffusion, the combination of the experimental studies on properties related to the diffusion and a first-principle molecular orbital calculation for cation-doped structures is effective. Recent studies on the TiO_2- or GeO_2-doped TZP showed that the superplastic flow stress correlates with the effective ionic bonding strength.[3,4] This result suggests that the grain boundary diffusivity of the Zr^{4+} cation in TZP may be closely related to the ionicity. However, the information is still limited, and further investigation is necessary to elucidate the origin of the doping effect on the grain boundary diffusion from an atomistic point of view. For this purpose, an ionic conductivity study by impedance spectroscopy should be adequate, because impedance spectroscopy may provide information on the matter transport through the grain interior and grain boundary.

The present study aims to investigate the effect of the 2 mol% TiO_2 and 2 mol% GeO_2 co-doping on the ionic conductivity of TZP. The doping effect on the chemical bonding state around the dopant cations was also investigated by a first-principle molecular orbital calculation in order to discuss the relationship between the atomic diffusion and chemical bonding state in the doped TZP.

2. Experimental procedures

2.1. Specimen preparation

The materials used were tetragonal ZrO_2 polycrystals (TZP) co-doped with 2 mol% TiO_2 and 2 mol% GeO_2. The starting powders were tetragonal ZrO_2 powders containing 3 mol%

* Corresponding author.
E-mail address: YOSHIDA.Hidehiro@nims.go.jp (H. Yoshida).

0955-2219/$ – see front matter © 2008 Elsevier Ltd. All rights reserved.
doi:10.1016/j.jeurceramsoc.2008.06.016

Table 1
Chemical compositions, sintering temperatures and average grain sizes of the undoped TZP, GeO_2-doped TZP and (TiO_2–GeO_2)-doped TZP

Specimen	Sintering temperature (°C)	Composition (mol%)			Grain size (μm)
		TZP	TiO_2	GeO_2	
TZP	1400	100	0	0	0.38
TZP + 2 mol% (TiO_2–GeO_2)	1300	96	2	2	0.35

Y_2O_3 (TZ3Y; Tosoh), TiO_2 (titanium (IV) oxide nanopowder, purity >99.9%, Aldrich) and GeO_2 (purity >99.999%, Rare Metallic). The TZP powders were mixed with the TiO_2 and GeO_2 powders and ball-milled for 24 h. The green compacts of TZP and the mixed powders were sintered at 1400 °C and 1300 °C, respectively, for 2 h in air. The chemical compositions and sintering temperatures of the present materials are listed in Table 1.

2.2. Microstructure analysis

The microstructures of the present materials were observed by scanning electron microscopy (SEM), conventional transmission electron microscopy (TEM) and high-resolution transmission electron microscopy (HRTEM). The average grain sizes of the present materials were measured by the linear intercept method using SEM photographs. The TEM specimens were prepared using standard techniques involving mechanical grinding to a thickness of less than 0.1 mm, and ion beam milling to an electron transparency at about 4 kV. For analysis of the Ti and Ge cation distributions in the TZP, scanning transmission electron microscopy (STEM) and an energy-dispersive X-ray spectroscopy (EDS) element mapping were also performed using the Noran Voyager system attached to a JEOL JEM-2010F field emission microscope with a focused beam size of about 1 nm.

2.3. Ionic conductivity

The ionic conductivity of the undoped and 2 mol% TiO_2–2 mol% GeO_2 co-doped TZP was measured by an AC impedance method (two-terminal).[8] The specimen sizes for the impedance measurements were $2.5 \times 2.5\ mm^2$ in electrode area s and 7 mm in length l, and platinum paste electrodes were joined on each end of the samples by firing at 930 °C for 15 min. The impedance spectra were obtained in air at temperatures ranging from 250 °C to 1000 °C over the frequency range from 0.1 MHz to 12 MHz at an applied voltage of 1 V using an impedance analyzer (Solartron SI 1260) with a resistance-heated furnace operated by zero-crossing power controls. The Z' and Z'' values in the complex impedance spectrum (Cole–Cole plot) are normalized by the division of l/s.

2.4. Molecular orbital calculation

A first-principle molecular orbital calculation was performed by self-consistently solving the Hartree–Fock–Slater equations using the discrete-variational (DV)-Xα method developed by Adachi et al.[9] In the DV-Xα method, numerical atomic orbitals obtained by solving the Schrödinger equation for atoms were used as the basic function. Fig. 1 shows the model cluster $[Y_4Zr_{18}O_{86}]^{-88}$ used for the calculation. In this cluster, two yttrium ions were substituted at the third nearest neighbor from a zirconium site Zr_1 as indicated in this figure. Based on the previous experimental and theoretical analyses,[10–14] an oxygen vacancy for maintaining electronic neutrality is introduced at the mutual second nearest neighbor sites from the two yttrium cations. Two other yttrium cations are also located at the third nearest neighbor sites from the Zr_2 site, and an oxygen vacancy is introduced at the second nearest neighbor from the two yttrium cations. The $[Y_4Zr_{16}Ti_2O_{86}]^{-88}$, $[Y_4Zr_{16}Ge_2O_{86}]^{-88}$ and $[Y_4Zr_{16}TiGeO_{86}]^{-88}$ model clusters, in which the Ti and/or Ge cations are substituted at the Zr_1 and

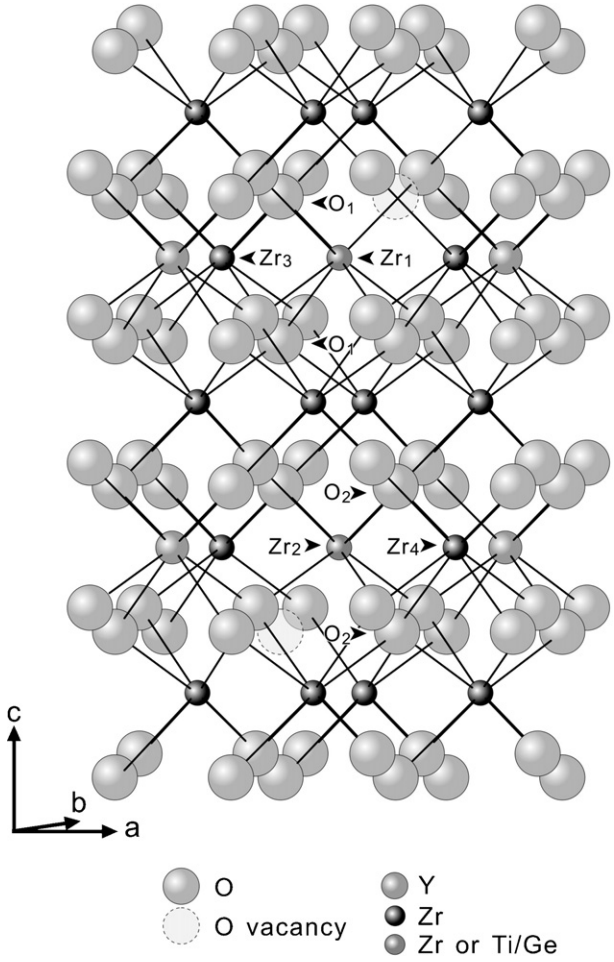

Fig. 1. Atomic structure of model cluster $[Y_4Zr_8O_{86}]^{-88}$.

Zr_2 sites, were made for the model clusters of the TiO_2-doped, GeO_2-doped and (TiO_2–GeO_2) co-doped TZPs, respectively. The model clusters were embedded in a field of Madelung potentials composed of 6000 point charges. Based on the Mulliken population analysis,[15] we can obtain information on the chemical bonding state, such as the bond overlap population between atoms (BOP), namely, the summation of the effective electron density in overlapping molecular orbitals between two atoms, and the electronic net charge for each atom (NC).[9] BOP and NC are regarded as indicators of the covalency between atoms and the effective ionic charge for each atom, respectively. In this study, we focused on the electronic state of the doped cations and the surrounding ions on the $(1\ \bar{1}\ 0)$ plane, namely, the nearest neighbor zirconium cation sites from Zr_1 and Zr_2 (Zr_3 and Zr_4, respectively), and the oxygen anions, O_1 and O_2, at the neighbor sites from the Zr_1 and Zr_3 cations and from the Zr_2 and Zr_4 cations, respectively, as indicated in Fig. 1.

3. Results

3.1. Microstructure

A relative density of about 99% and an average grain size of about 0.4 μm were obtained in the sintered materials. The average grain sizes of the present materials in the as-sintered condition are listed in Table 1. Fig. 2 shows an example of the SEM images in the as-sintered (a) undoped TZP and (b) 2 mol% TiO_2 and 2 mol% GeO_2 (2 mol% (TiO_2–GeO_2))-doped TZP. Uniform and equiaxed grain structures without residual pores were obtained in the present materials. As compared to the undoped TZP, the (TiO_2–GeO_2)-doped TZP reached the same relative density at the lower sintering temperature of 1300 °C. This fact suggests that the atomic diffusion in TZP was enhanced by the (TiO_2–GeO_2)-doping at the sintering temperature. The materials doped with TiO_2 and GeO_2 had a monolithic microstructure consisting of equiaxed zirconia grains in the SEM images. The monolithic microstructure in the (TiO_2–GeO_2)-doped TZP has also been confirmed by high-resolution TEM observations. Fig. 3 shows a typical HRTEM image of a grain boundary in 2 mol% (TiO_2–GeO_2)-doped TZP. The lattice fringes can be seen for two grains, and no second phase particle or amorphous

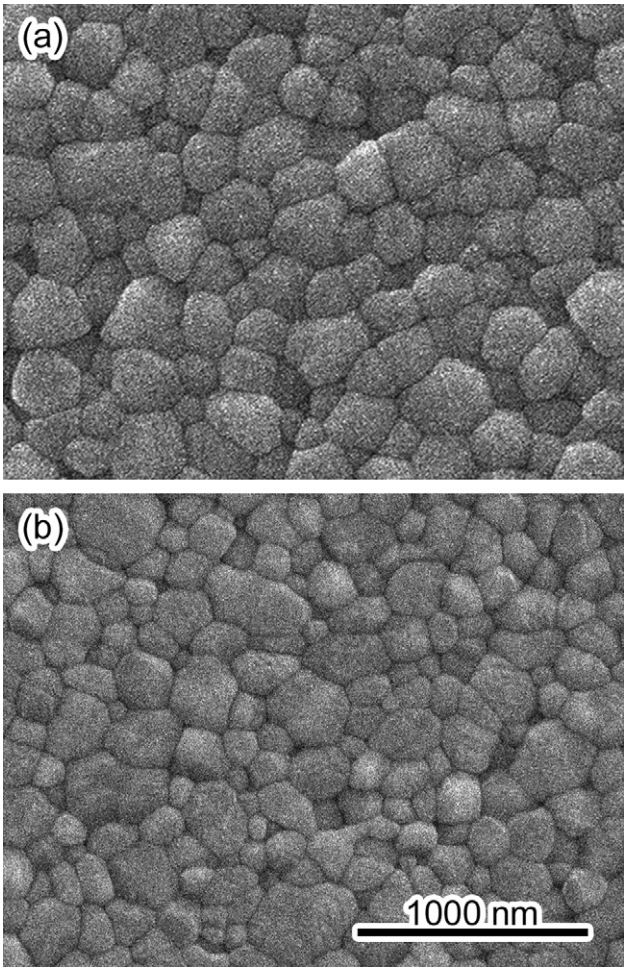

Fig. 2. Scanning electron microscopy images of (a) the undoped TZP and (b) 2 mol% TiO_2 and 2 mol% GeO_2 co-doped TZP.

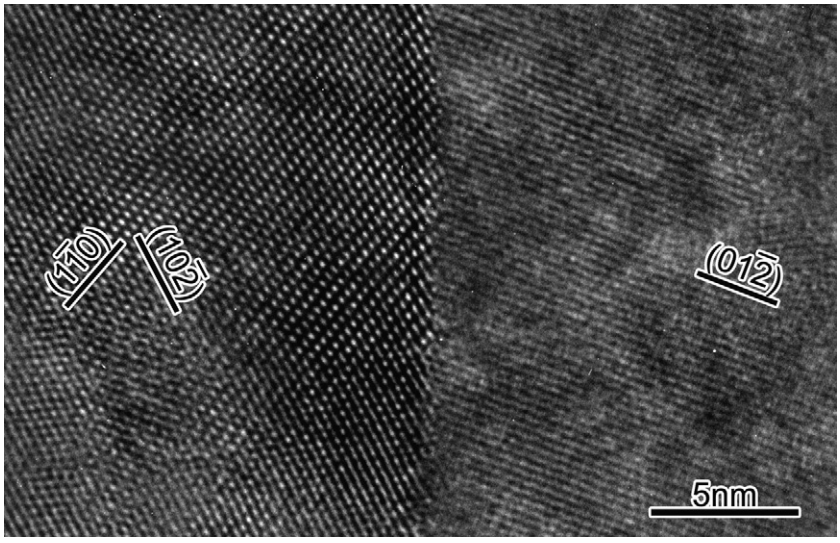

Fig. 3. A high-resolution transmission electron microscopy image of a grain boundary in 2 mol% TiO_2–2 mol% GeO_2 co-doped TZP.

layer exists along the grain boundary; the two grains are directly bonded at the boundary. The monolithic microstructure indicates that the doped cations segregate along the grain boundaries and/or dissolved in the matrix grains.

EDS elemental mapping using STEM with a focused electron beam size of about 1 nm was performed to examine the distribution of the dopant cations in the (TiO_2–GeO_2)-doped TZP. Fig. 4 shows (a) a bright field image, (b) Ti Kα and (c) Ge Kα mapping images for the grain boundaries in the 2 mol% (TiO_2–GeO_2)-doped TZP. While the (TiO_2–GeO_2)-doped TZP exhibits a single-phase microstructure, the Ti and Ge cations exist in a high concentration along the grain boundaries of the TZP as shown in Fig. 4(b) and (c). The present HRTEM observations and STEM–EDS measurements indicate that the doped cations tend to segregate along the grain boundaries in the TZP, and not form an amorphous layer or second phase particle. The present results are consistent with the previous studies that revealed the grain boundary segregation of the dopant cations.[1,2,16–18]

3.2. Ionic conductivity

Fig. 5 shows examples of the complex impedance spectra (Cole–Cole plots) at 450 °C for the undoped and 2 mol% (TiO_2–GeO_2)-doped TZPs. The spectrum for the (TiO_2–GeO_2)-doped TZP can be resolved into two semicircles and part of an electrode arc which extends below the employed frequency range. The left semicircle at the higher frequency and the right semicircle at the lower frequency are attributed to the grain interior and grain boundary contributions, respectively.[18,19] The intersections of the extrapolated lines of the semicircles with the Z'-axis give the resistivities originating from the grain interior and the grain boundary of the sample. The results in Fig. 5 also clearly indicate that the resistivity of TZP was significantly increased by the (TiO_2–GeO_2)-doping. The existence of the electrode arc in the present samples suggests that the conductivity was essentially ionic.[20]

In order to obtain the activation energy for the conductivity, the equation for the ionic conductivity usually applied to a doped oxide conductor is given by

$$\sigma T = A \exp\left[\frac{-\Delta H}{kT}\right]$$

where σ is the conductivity at absolute temperature T, A is the pre-exponential factor, ΔH is the activation energy for the conductivity, and k is Boltzmann's constant.[21] Fig. 6 shows the Arrhenius plot of the total conductivity in the undoped TZP and 2 mol% (TiO_2–GeO_2)-doped TZPs. In Fig. 6, previous data for the 3 mol% Y_2O_3-stabilized TZP are also plotted for comparison.[22] The data for the TZP in the present study agree well with the previous ones. On the other hand, the total conductivity of TZP decreases due to the (TiO_2–GeO_2)-doping. It has been reported that the ionic conductivity in air of TZP decreases with a 1–20 mol% TiO_2 addition.[22,23] The present result indicates that the (TiO_2–GeO_2)-doping also decreases the conductivity. The present data for the TZP do not show a single linear relationship, but consists of two linear regions with slightly different slopes; the total conductivity

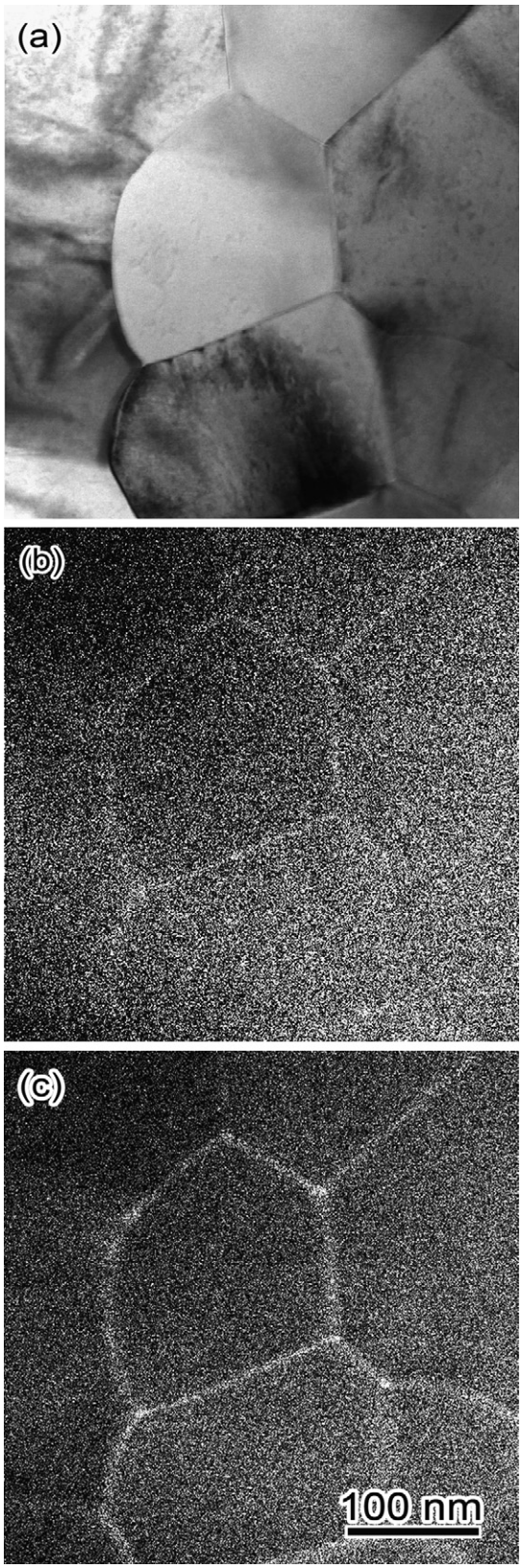

Fig. 4. (a) A bright field TEM image, and (b) Ti Kα and (c) Ge Kα mapping images obtained by STEM-nanoprobe EDS technique for grain boundaries in 2 mol% TiO_2 and 2 mol% GeO_2 co-doped TZP.

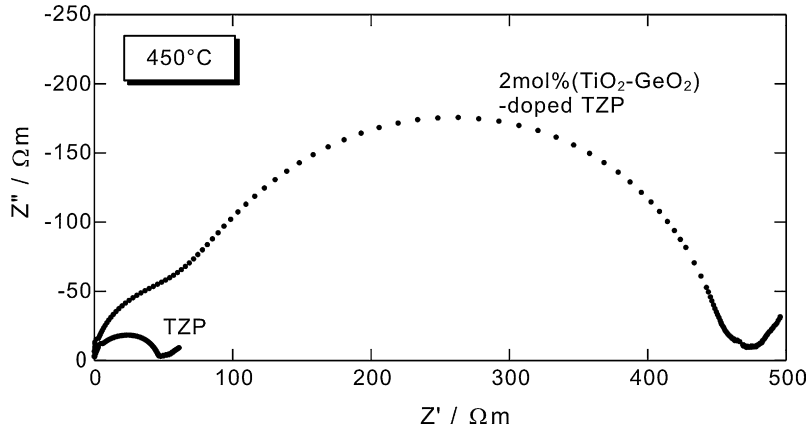

Fig. 5. Complex impedance spectra at 450 °C of the undoped TZP and 2 mol% TiO_2–2 mol% GeO_2 co-doped TZP.

in the TZP exhibits a lower value for the slope at temperatures over 800 °C. High temperature bending has also been observed in the literature.[24]

In the ZrO_2–Y_2O_3 system, the contribution of the oxygen anion to the total conductivity of a solid electrolyte is higher than 99%; the ion transference number is greater than 0.99.[25] The conductivity of the present materials can therefore be regarded as the oxygen anion conductivity. The activation energy for the ionic conduction is expressed as the summation of the binding enthalpy of the association of an oxygen vacancy and a cation $(Y'_{Zr}V^{\cdot\cdot}_{O})^{\cdot}$, and the enthalpy of the oxygen anion vacancy motion.[21,26–28] The effect of the binding enthalpy of the associate can significantly influence the population of free vacancies at temperatures below 800 °C, but the complex of $(Y'_{Zr}V^{\cdot\cdot}_{O})^{\cdot}$ completely dissociates to free $V^{\cdot\cdot}_{O}$ and Y'_{Zr} at the higher temperatures.[27,28] Therefore, the migration enthalpy of the oxygen anion can be estimated from the slope of the temperature dependence for conduction over 800 °C. The values of the activation energy in the undoped TZP at high (>800 °C) and low (<750 °C) temperatures are 76 kJ/mol and 93 kJ/mol, respectively. On the other hand, the slope of the data in the (TiO_2–GeO_2)-doped TZP slightly decreases over 850 °C, and the activation energies for the total conductivity at high and low temperatures are 98 kJ/mol and 108 kJ/mol, respectively. In other words, the values of the binding enthalpy of the association in the undoped TZP and (TiO_2–GeO_2)-doped TZP are 17 kJ/mol and 10 kJ/mol, respectively. It has been reported that the association enthalpy in the 4.8 mol% Y_2O_3-doped ZrO_2 consisting of tetragonal and cubic phases is about 12 kJ/mol.[29] The present association enthalpy data for the TZP is close to the reported value. The increased migration enthalpy values indicate that the retarded oxygen anion's diffusion occurs due to the (TiO_2–GeO_2)-doping, which corresponds to a lower conductivity of the (TiO_2–GeO_2)-doped TZP than that of the undoped TZP.

Fig. 7 shows the Arrhenius plot of the grain interior and grain boundary conductivity in the undoped TZP and 2 mol% (TiO_2–GeO_2)-doped TZP. Because the semicircles attributed to

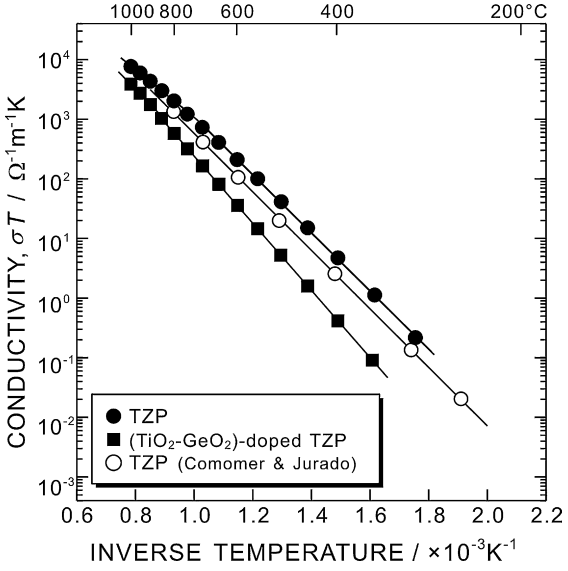

Fig. 6. Arrhenius plots of the total conductivity of the undoped and 2 mol% (TiO_2–GeO_2) co-doped TZP. The previous data for 3 mol%Y_2O_3-stabilized TZP[22] are also plotted for comparison.

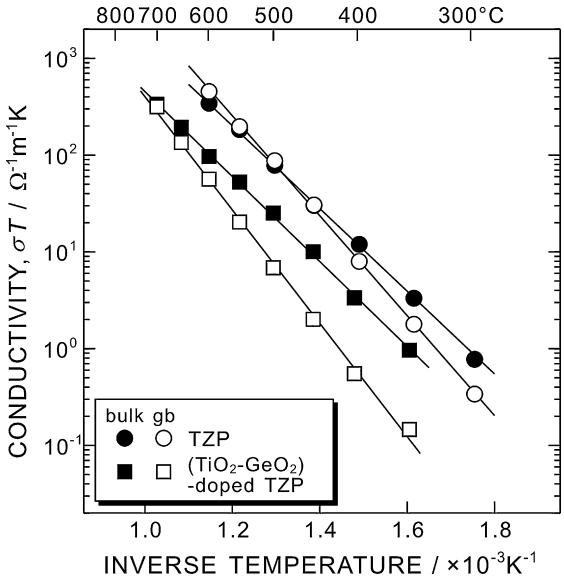

Fig. 7. Arrhenius plots of the grain interior (bulk) and grain boundary (gb) conductivity of the undoped TZP and 2 mol% (TiO_2–GeO_2) co-doped TZP.

Table 2
The activation energy values of grain interior conductivity E_{bulk} and grain boundary conductivity E_{gb} in TZP and (TiO_2–GeO_2)-doped TZP

Sample	E_{bulk} (kJ/mol)	E_{gb} (kJ/mol)	Reference
TZP	85	94	Present work
(TiO_2–GeO_2) co-doped TZP	88	112	Present work
3 mol% Y_2O_3-stabilized TZP	88.8	105	Bonanos et al.[20]
3 mol% Y_2O_3-stabilized TZP	82	N/A	Colomer and Jurado[22]
3 mol% Y_2O_3-stabilized TZP	82.9	97.4	Durán et al.[23]
3 mol% Y_2O_3-stabilized TZP	86.3	98.3	Sakka et al.[31]

the grain interior and grain boundary contributions cannot be clearly identified at high temperatures, the data are plotted in the temperature range of 300–700 °C. The data for the undoped TZP are close to the reported ones.[30,31] Both the grain interior and grain boundary conductivities are lower in the (TiO_2–GeO_2)-doped TZP than in the undoped TZP. The activation energy values for the grain interior conductivity (E_{bulk}) and grain boundary conductivity (E_{gb}) in the undoped and co-doped TZPs are summarized in Table 2. The corresponding values for the previously reported 3 mol% Y_2O_3-stabilized TZP[20,22,23,31] are also included for comparison. The values of the activation energy of the grain interior and grain boundary are in good agreement with those reported for TZP. The slightly higher E_{gb} value reported by Bonanos et al. may be due to differences in the impurity level and/or the relative density; for instance, the value of E_{gb} increases due to the presence of residual pores at the grain boundary. On the other hand, the activation energy is increased by the (TiO_2–GeO_2)-doping. The data in Fig. 7 indicate that the (TiO_2–GeO_2)-doping results in a decreasing conductivity within the grains and along the grain boundaries, leading to an overall conductivity reduction of about one order of magnitude in comparison to the TZP. Because the association enthalpy is relatively low when compared to the migration enthalpy (Fig. 6), the decreasing conductivity and increasing activation energy are caused by retardation of the oxygen anion's diffusion. The reduced grain boundary conductivity of the oxygen anion and the increased activation energy in the (TiO_2–GeO_2)-doped TZP are ascribed to the intergranular segregation of the Ti and Ge cations.

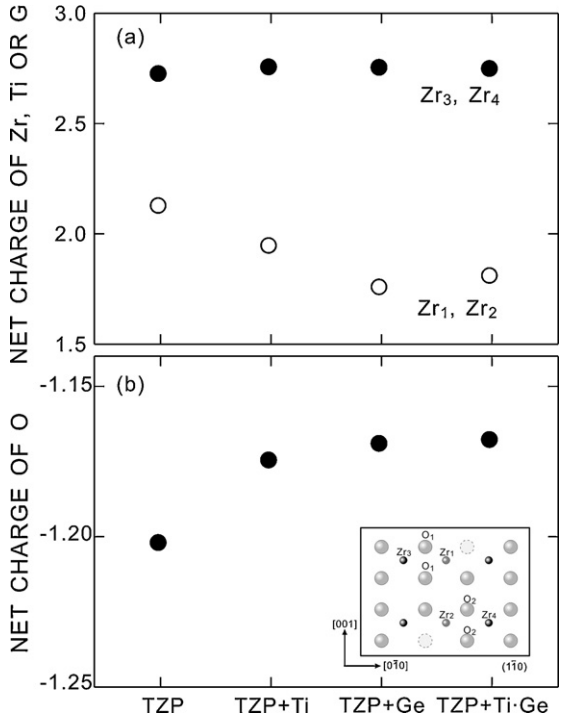

Fig. 8. Average values of net charges in (a) Zr, Ti and/or Ge cations at either the (Zr_1, Zr_2) sites or (Zr_2, Zr_4) sites and (b) O anions at the O_1 and O_2 sites for the four model clusters.

3.3. Molecular orbital calculation

Fig. 8 shows the average NC values of (a) the Zr, Ti or Ge cations at the Zr_1 and Zr_2 sites (open circles), Zr cations at the Zr_3 and Zr_4 sites (closed circles), and (b) the neighboring O anions from the Zr_1 and Zr_3 sites (O_1) and from the Zr_2 and Zr_4 sites (O_2) for the four model clusters. Due to the oxygen vacancies for the neighbors of the Zr_1 and Zr_2 sites, the NC values of Zr_1 and Zr_2 are lower than those of Zr_3 and Zr_4. The NC values of Zr_1 and Zr_2 in the Ti- and/or Ge-doped clusters are lower than those of the Zr cations in the TZP cluster, whereas those of Zr_3 and Zr_4 are almost unchanged in the Ti- and/or Ge-doped clusters. On the other hand, the NC values of the O anions in the Ti- and/or Ge-doped clusters are higher than those in the undoped TZP cluster; that is, the ionicity of the oxygen anions is decreased in the neighborhood of the Ti and Ge cations.

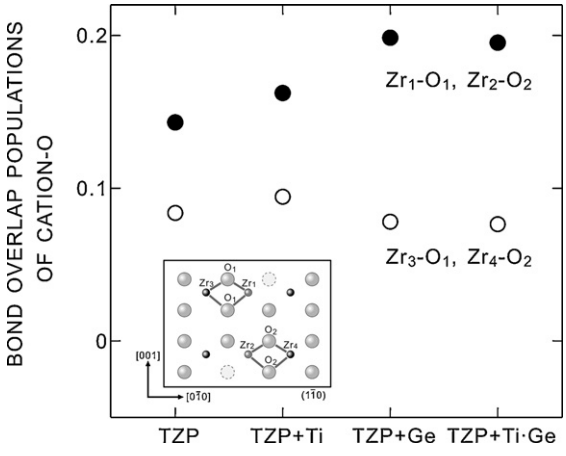

Fig. 9. Average values of bond overlap populations of either the (Zr_1–O_1, Zr_2–O_2) bonds or (Zr_3–O_1, Zr_4–O_2) bonds for the four model clusters.

Fig. 9 shows the average BOPs of the (Zr_1–O_1, Zr_2–O_2) bonds (closed circles) and (Zr_3–O_1, Zr_4–O_2) bonds (open circles) for the four model clusters. In the (Zr_1–O_1, Zr_2–O_2) bonds, the Ti–O and Ge–O bonds of the Ti- and/or Ge-doped clusters have higher BOPs than the (Zr_1–O_1, Zr_2–O_2) bonds in the TZP cluster, whereas the BOPs of the (Zr_3–O_1, Zr_4–O_2) bonds are only slightly changed by the Ti and/or Ge-doping. The Ge-doping significantly increases the BOP value for the (Zr_1–O_1, Zr_2–O_2) bonds. This result indicates that the Ti–O and Ge–O bonds have a higher covalency than the Zr–O bonds. The lower ionicity of the Ti- and/or Ge-doped TZPs is due to the formation of stronger covalent bonds with the oxygen anions. The substitution of the Ti and/or Ge cations for the Zr cations strongly influences the chemical bonding states of, in particular, the nearest neighbor oxygen anions.

4. Discussion

The results in Figs. 6 and 7 indicate that the grain boundary diffusion of oxygen anions in the TZP is retarded by the grain boundary segregation of TiO_2–GeO_2. In addition, the molecular orbital calculation indicates that the substitution of the Ti and Ge cations for Zr cations increases the covalent bond strength between the dopant cations and the nearest neighbor oxygen anions. The molecular orbital calculation provides a reasonable estimation of the change in the electronic state due to the Ti- and Ge-doping. Because the energy levels of the outer shells of electrons are lower in a Ti atom and are much lower in a Ge atom as compared to those in a Zr atom,[32] the polarity of the cation–anion bonds decreases, and therefore their covalency should increase[33] when compared to that of the undoped TZP.

According to an X-ray absorption spectroscopy (XAS) analysis of the atomic configuration in 5 mol% or 10 mol% TiO_2-TZP solid solution,[23] the Ti–O bond is shorter than the Zr–O bond in the TZP. The earlier studies of the TiO_2-added TZP concluded that the ionic conductivity reduced by the 5–20 mol% TiO_2 addition results from a loss of centrosymmetry in the TZP.[23] In addition, an XAS analysis of the 5–15 mol% GeO_2-added ZrO_2 also indicates that the Ge–O bond is shorter than the Zr–O bond.[10] From a classical point of view, an undersized cation such as Ge^{4+} and Ti^{4+} in ZrO_2 must draw neighboring oxygen anions toward the dopant cation itself, and thereby suppresses the oxygen anion diffusion. This corresponds to the formation of the strong covalent bond between the Ti/Ge cations and O anions. Fig. 10 is a schematic illustration of the chemical bonding state in the TZP doped with the Ge^{4+} or Ti^{4+} cation. On the basis of Pauling's electronegativity scale, the fraction of ionic character of the Zr–O bond is about 60%.[34] This estimation means that the ionic bond is probably a major part of the binding force of ZrO_2, but the covalency also provides a significant contribution. The molecular orbital calculations indicate that the Ti/Ge cations and the surrounding O anions form strong covalent bonds, whereas the covalent bonds between the Zr cations and O anions are unchanged. The formation of the strong covalent bonds must retard the oxygen anion diffusion. Since the covalent bond is strong with a spatial anisotropic binding in comparison to an ionic bond,[33] the increased covalent bonding strength due to the grain boundary segregation of the Ge cations, in particular, effectively reduces the value of the oxygen anion's diffusivity. On the other hand, the ionicity of the neighboring oxygen anions is reduced by the Ti and Ge cations, whereas the ionicity of the Zr cations at the Zr_3 and Zr_4 sites is only slightly changed. The reduction in the ionic bonds between the oxygen anion and zirconium cation probably causes the enhanced diffusion of the Zr cation, which has been suggested by the data for the superplastic flow in the (TiO_2–GeO_2)-doped TZP.[3]

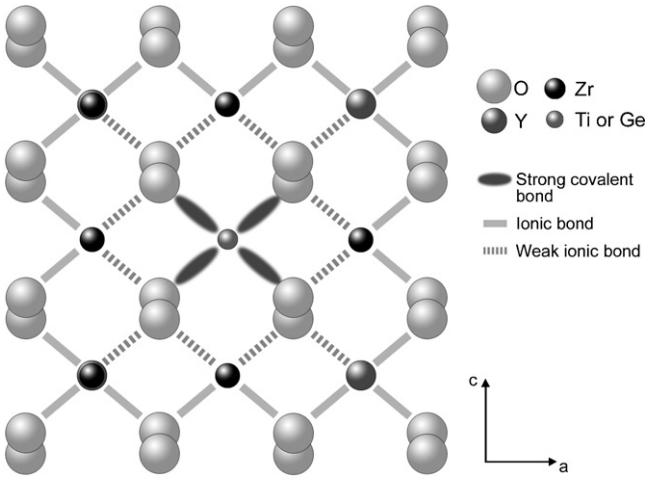

Fig. 10. A schematic illustration of chemical bonding state in Ti- or Ge-doped TZP.

5. Conclusions

In yttria-stabilized tetragonal zirconia, the co-doping of 2 mol% TiO_2 and 2 mol% GeO_2 causes the segregation of Ti^{4+} and Ge^{4+} cations along the grain boundaries. This segregation causes a reduction in the conductivity of both the grain interior and grain boundary and an increase in the activation energy for the grain boundary conductivity. The conductivity data indicate that the segregation retards the diffusion of oxygen anions. The first-principle molecular orbital calculation for a doped model cluster suggests that the retarded oxygen diffusion along the grain boundary can be ascribed to the change in the covalent bonds around the doped cations; the formation of the strong covalent bond between oxygen and the doped cation should suppress the diffusion of the oxygen anion.

Acknowledgements

The authors wish to express their gratitude to the Ministry of Education, Culture, Sports, Science and Technology and the Japan Society for the Promotion of Science for their financial support by a Grant-in-Aid for Encouragement of Young Scientists (19686042). We also wish to express our thanks to the Iketani Science and Technology Foundation for their financial aid.

References

1. Mimurada, J., Nakano, M., Sasaki, K., Ikuhara, Y. and Sakuma, T., Effect of cation doping on the superplastic flow in yttria-stabilized

tetragonal zirconia polycrystals. *J. Am. Ceram. Soc.*, 2001, **84**, 1817–1821.
2. Nakatani, K., Nagayama, H., Yoshida, H., Yamamoto, T. and Sakuma, T., The effect of grain boundary segregation on superplastic behavior in cation-doped 3Y-TZP. *Scripta Mater.*, 2003, **49**, 791–795.
3. Yoshida, H., Doping dependence of high temperature plastic flow behavior in TiO_2- and GeO_2-doped tetragonal ZrO_2 polycrystals. *J. Ceram. Soc. Jpn.*, 2006, **114**, 155–160.
4. Kuwabara, A., Nakano, M., Yoshida, H., Ikuhara, Y. and Sakuma, T., Superplastic flow stress and electronic structure in yttria-stabilized tetragonal zirconia polycrystals doped with GeO_2 and TiO_2. *Acta Mater.*, 2004, **52**, 5563–5569.
5. Chokshi, A. H., Mukherjee, A. K. and Langdon, T. G., Superplasticity in advanced materials. *Mater. Sci. Eng. R*, 1993, **10**, 237–274.
6. Jiménez-Melendo, M., Domínguez-Rodríguez, A. and Bravo-León, A., Superplastic flow of fine-grained yttria-stabilized zirconia polycrystals: constitutive equation and deformation mechanisms. *J. Am. Ceram. Soc.*, 1998, **81**, 2761–2776.
7. Owen, D. M. and Chokshi, A. H., The high temperature mechanical characteristics of superplastic 3 mol% yttria stabilized zirconia. *Acta Mater.*, 1998, **46**, 667–679.
8. Bauerle, J. E., Study of solid electrolyte polarization by a complex admittance method. *J. Phys. Chem. Solids*, 1969, **30**, 2657–2670.
9. Adachi, H., Tsukada, M. and Satoko, C., Discrete variational X-alpha cluster calculations. 1. Application to metal clusters. *J. Phys. Soc. Jpn.*, 1978, **45**, 875–883.
10. Li, P., Chen, I.-W. and Penner-Hahn, J. E., Effect of dopants on zirconia stabilization—an X-ray absorption study. II. Tetravalent dopants. *J. Am. Ceram. Soc.*, 1994, **77**, 118–128.
11. Zacate, M. O., Minervini, L., Bradfield, D. J., Grimes, R. W. and Sickafus, K. E., Defect cluster formation in M_2O_3-doped cubic ZrO_2. *Solid State Ionics*, 2000, **128**, 243–254.
12. Khan, M. S., Islam, M. S. and Bates, D. R., Cation doping and oxygen diffusion in zirconia: a combined atomistic simulation and molecular dynamics study. *J. Mater. Chem.*, 1998, **8**, 2299–2307.
13. Stapper, G., Bernasconi, M., Nicoloso, N. and Parrinello, M., Ab initio study of structural and electronic properties of yttria-stabilized cubic zirconia. *Phys. Rev. B*, 1999, **59**, 797–810.
14. Bogicevic, A., Wolverton, C., Crosbie, G. M. and Stechel, E. B., Defect ordering in aliovalently doped cubic zirconia from first principles. *Phys. Rev. B*, 2001, **64**, 014106/1-14.
15. Mulliken, R. S., Electronic population analysis on LCAO-MO molecular wave functions. 1. *J. Chem. Phys.*, 1955, **23**, 1833–1840.
16. Aoki, M., Chiang, Y.-M., Kosacki, I., Lee, J.-R., Tuller, H. and Liu, Y., Solute segregation and grain-boundary impedance in high-purity stabilized zirconia. *J. Am. Ceram. Soc.*, 1996, **79**, 1169–1180.
17. Chokshi, A. H., Yoshida, H., Ikuhara, Y. and Sakuma, T., The influence of trace elements on grain boundary processes in yttria-stabilized tetragonal zirconia. *Mater. Lett.*, 2003, **57**, 4196–4201.
18. Morita, K., Hiraga, K. and Kim, B.-N., Effect of minor SiO_2 addition on the creep behavior of superplastic tetragonal ZrO_2. *Acta Mater.*, 2004, **52**, 3355–3364.
19. Badwal, S. P. S., Effect of dopant concentration on the grain boundary and volume resistivity of yttria–zirconia. *J. Mater. Sci. Lett.*, 1987, **6**, 1419–1421.
20. Bonanos, N., Slotwinski, R. K., Steele, B. C. H. and Butler, E. P., High ionic-conductivity in polycrystalline tetragonal Y_2O_3–ZrO_2. *J. Mater. Sci. Lett.*, 1984, **3**, 245–248.
21. Kilner, J. A. and Brook, R. J., A study of oxygen ion conductivity in doped non-stoichiometric oxides. *Solid State Ionics*, 1982, **6**, 237–252.
22. Colomer, M. T. and Jurado, J. R., Structure, microstructure and mixed conduction of $[(ZrO_2)_{092}(Y_2O_3)_{0.08}]_{0.9}(TiO_2)_{0.1}$. *J. Solid State Chem.*, 2002, **165**, 79–88.
23. Durán, P., Capel, F., Moure, C., González-Elipe, A. R., Caballero, A. and Bañares, M. A., Mixed (oxygen ion and n-type) conductivity and structural characterization of titania-doped stabilized tetragonal zirconia. *J. Electrochem. Soc.*, 1999, **146**, 2425–2434.
24. Sakka, Y., Suzuki, T. S., Matsumoto, T., Morita, K., Hiraga, K. and Moriyoshi, Y., Effect of titania and magnesia addition to 3 mol% yttria doped tetragonal zirconia on some diffusion related phenomena. *Solid State Ionics*, 2004, **172**, 499–503.
25. Kilner, J. A. and Steele, C. H., Mass transport in anion-deficient fluorite oxides. In *Nonstoichiometric Oxides*, ed. O. Toft Sørensen. Academic Press, New York, 1981, p. 233.
26. Kilner, J. A. and Waters, C. D., The effect of dopant cation–oxygen vacancy complexes on the anion transport properties of non-stoichiometric fluorite oxides. *Solid State Ionics*, 1982, **6**, 253–259.
27. Arachi, Y., Sakai, H., Yamamoto, O., Takeda, Y. and Imanishi, N., Electrical conductivity of the ZrO_2–Ln_2O_3 (Ln = lanthanoides) system. *Solid State Ionics*, 1999, **121**, 133–139.
28. Kharton, V. V., Marques, F. M. B. and Atkinson, A., Transport properties of solid oxide electrolyte ceramics: a brief review. *Solid State Ionics*, 2004, **174**, 135–149.
29. Jie, L., Almond, D. P. and Stevens, R., Ionic mobilities and association energies from an analysis of electrical impedance of ZrO_2–Y_2O_3 alloys. *J. Am. Ceram. Soc.*, 2000, **83**, 1703–1708.
30. Gödickemeier, M., Michel, B., Orliukas, A., Bohac, P., Sasaki, K., Gauckler, L., Heinrich, H., Schwander, P., Kostorz, G., Hofmann, H. and Frei, O., Effect of intergranular glass films on the electrical conductivity of 3Y-TZP. *J. Mater. Res.*, 1994, **9**, 1228–1240.
31. Sakka, Y., Suzuki, T. S., Ozawa, K., Uchikoshi, T. and Hiraga, K., Sintering and ionic conductivity of CuO-doped tetragonal ZrO_2 prepared by novel colloidal processing. *J. Ceram. Soc. Jpn.*, 2001, **109**, 1004–1009.
32. Herman, F. and Skillman, S., *Atomic Structure Calculations*. Prentice-Hall, Englewood Cliffs, NJ, 1963, pp. 2/1–2/17.
33. Harrison, W. A. and Electronic, *Structure and the Properties of Solids*. Dover Publications, New York, 1989, pp. 32–46.
34. Kingery, W. D., Bowen, H. K. and Uhlmann, D. R., *Introduction to Ceramics*. A Wiley–Interscience Publication, John Wiley and Sons, New York, 1976, pp. 36–40.